

Hybrid LDA and generalized tight-binding method for electronic structure calculations of strongly correlated electron systems

M. M. Korshunov,* V. A. Gavrichkov, and S. G. Ovchinnikov

*L.V. Kirensky Institute of Physics, Siberian Branch of Russian Academy of Sciences, 660036 Krasnoyarsk, Russia*I. A. Nekrasov, Z. V. Pchelkina,[†] and V. I. Anisimov*Institute of Metal Physics, Russian Academy of Sciences-Ural Division, 620219 Yekaterinburg GSP-170, Russia*

(Received 6 May 2005; revised manuscript received 11 August 2005; published 7 October 2005)

A hybrid scheme for the electronic structure calculations of strongly correlated electron systems is proposed. The *ab initio* local density approximation calculation is used to construct the Wannier functions and obtain single electron and Coulomb parameters of the multiband Hubbard-type model. In strong correlation regime the electronic structure within multiband Hubbard model is calculated by the generalized tight-binding method, which combines the exact diagonalization of the model Hamiltonian for a small cluster (unit cell) with perturbation treatment of the intercluster hopping and interactions. For undoped La_2CuO_4 and Nd_2CuO_4 this scheme results in charge transfer insulators with correct values of gaps and dispersions of bands in agreement with the angle-resolved photoemission data.

DOI: [10.1103/PhysRevB.72.165104](https://doi.org/10.1103/PhysRevB.72.165104)

PACS number(s): 74.72.-h, 74.20.-z, 74.25.Jb, 31.15.Ar

I. INTRODUCTION

A conventional band theory is based on the density functional theory¹ (DFT) and on the local density approximation² (LDA) within DFT. In spite of great success of the LDA and its extensions for conventional metallic systems it appears to be inadequate for strongly correlated electron systems (SCES). For instance, LDA predicts La_2CuO_4 to be a metal whereas, in reality, it is an insulator. Several approaches to include strong correlations in the LDA method are known, for example, LDA+U (Ref. 3) and LDA-SIC.⁴ Both methods result in the correct antiferromagnetic insulator ground state for La_2CuO_4 contrary to LDA, but the origin of the insulating gap is not correct. It is formed by the local single-electron states splitted by spin or orbital polarization. In these approaches the paramagnetic phase of the undoped La_2CuO_4 (above the Néel temperature T_N) will be metallic in spite of strong correlation regime $U \gg W$, where U is the Hubbard Coulomb parameter⁵ and W is a free electron bandwidth. The spectral weight redistribution between Hubbard subbands is very important effect in SCES that is related to the formation of the Mott-Hubbard gap in the paramagnetic phase. This effect is incorporated in the hybrid LDA+dynamical mean field theory (DMFT) (for review see Refs. 6–9) and LDA++ approaches.⁹ The electron self-energy in LDA+DMFT approach is calculated by the DMFT theory in the limit of infinite dimension^{10,11} and is \mathbf{k} independent, $\Sigma_{\mathbf{k}}(E) \rightarrow \Sigma(E)$.^{12,13} That is why the correct band dispersion and the ARPES data for high- T_c compounds cannot be obtained within LDA+DMFT theory. Recent development of the LDA+cluster DMFT method^{14,15} and spectral density functional theory¹⁶ gives some hope that nonlocal corrections may be included in this scheme. Another self-consistent scheme with advantage to be valid for excited states in contrast with standard DFT calculations is known as GW approximation.^{17,18} The GW method now is a fully working method for electronic structure calculations^{19,20} taking into

account electron correlations. Recently it was successfully applied to some strongly correlated materials.²¹

A generalized tight-binding²² (GTB) method has been proposed to study the electronic structure of SCES as a generalization of Hubbard ideas for the realistic multiband Hubbard-like models. The GTB method combines the exact diagonalization of the intracell part of the Hamiltonian, construction of the Hubbard operators on the basis of the exact intracell multielectron eigenstates, and the perturbation treatment of the intercell hoppings and interactions. A similar approach to the three-band *p-d* model of cuprates^{23,24} is known as the cell perturbation method.^{25–27} The practical realization of the GTB method for cuprates required an explicit construction of the Wannier functions to overcome the non-orthogonality of the oxygen molecular orbitals at the neighboring CuO_6 cells.²⁸ The GTB calculations for undoped and underdoped cuprates are in good agreement with angle-resolved photoemission (ARPES) data both in the dispersion of the valence band and in the spectral intensity.^{28,29} A strong redistribution of spectral weight with hole doping and the formation of the in-gap states have been obtained in these calculations. Similar GTB calculations for the manganites has been done recently.³⁰

As any model Hamiltonian approach the GTB method is not *ab initio*, there are many Hamiltonian parameters such as intra-atomic energy levels of *p* and *d* electrons, various *p-d* and *p-p* hopping parameters, Coulomb and exchange interaction parameters. These parameters have been obtained by fitting the set of optical, magnetic³¹ and ARPES data.²⁸ Generally the question arises how unique the set of parameters is. To overcome this restriction we have proposed in this paper a hybrid LDA+GTB scheme that allows one to calculate the GTB parameters by the *ab initio* LDA approach.

The paper is organized as follows. In Sec. II the construction of Wannier functions from self-consistent LDA eigenfunctions as well as *ab initio* parameters of the multiband *p-d* model for La_2CuO_4 and Nd_2CuO_4 are given. A brief

description of the GTB method is done in Sec. III. Section IV contains the LDA+GTB band structure calculations for La_2CuO_4 and Nd_2CuO_4 . The effective low-energy t - J^* model with *ab initio* parameters is presented in Sec. V. Section VI is the conclusion.

II. CALCULATION OF *AB INITIO* PARAMETERS FROM LDA

To obtain hopping integrals for different sets of bands included in consideration we apply projection procedure using Wannier functions (WFs) formalism.³⁶ WFs were first introduced in 1937 by Wannier³² as Fourier transformation of Bloch states $|\psi_{i\mathbf{k}}\rangle$

$$|W_i^{\mathbf{T}}\rangle = \frac{1}{\sqrt{N}} \sum_{\mathbf{k}} e^{-i\mathbf{k}\cdot\mathbf{T}} |\psi_{i\mathbf{k}}\rangle, \quad (1)$$

where \mathbf{T} is lattice translation vector, N is the number of discrete \mathbf{k} points in the first Brillouin zone, and i is band index. One major reason why the WFs have seen little practical use in solid-state applications is their nonuniqueness since for a certain set of bands any orthogonal linear combination of Bloch functions $|\psi_{i\mathbf{k}}\rangle$ can be used in Eq. (1). Therefore to define them one needs an additional constraint. Among others, Marzari and Vanderbilt³³ proposed the condition of maximum localization for WFs, resulting in a variational procedure. To get a good initial guess authors of Ref. 33 proposed to choose a set of localized trial functions $|\phi_n\rangle$ and project them onto the Bloch states $|\psi_{i\mathbf{k}}\rangle$. It was found that this starting guess is usually quite good. This fact later led to the simplified calculating scheme³⁴ where the variational procedure was abandoned as in the present work and the result of the aforementioned projection was considered as the final step.

A. Wannier function formalism

To construct the WFs one should define a set of trial orbitals $|\phi_n\rangle$ and choose the Bloch functions of interest by band indexes (N_1, \dots, N_2) or by energy interval (E_1, E_2). Nonorthogonalized WFs in reciprocal $|\tilde{W}_{n\mathbf{k}}\rangle$ space are then the projection of the set of site-centered atomiclike trial orbitals $|\phi_n\rangle$ on the Bloch functions $|\psi_{i\mathbf{k}}\rangle$ of the chosen bands:

$$|\tilde{W}_{n\mathbf{k}}\rangle \equiv \sum_{i|E_1 \leq \epsilon_i(\mathbf{k}) \leq E_2} |\psi_{i\mathbf{k}}\rangle \langle \psi_{i\mathbf{k}} | \phi_n \rangle, \quad (2)$$

where $\epsilon_i(\mathbf{k})$ is the band dispersion of i th band obtained from self-consistent *ab initio* LDA calculation. In the present work we use LMT orbitals³⁵ as trial functions. The Bloch functions in LMTO basis are defined as

$$|\psi_{i\mathbf{k}}\rangle = \sum_{\mu} c_{\mu i}^{\mathbf{k}} |\phi_{\mu}^{\mathbf{k}}\rangle, \quad (3)$$

where μ is the combined index representing qlm (q is the atomic number in the unit cell, l and m are orbital and magnetic quantum numbers), $\phi_{\mu}^{\mathbf{k}}(\mathbf{r})$ are the Bloch sums of the basis orbitals $\phi_{\mu}(\mathbf{r}-\mathbf{T})$

$$\phi_{\mu}^{\mathbf{k}}(\mathbf{r}) = \frac{1}{\sqrt{N}} \sum_{\mathbf{T}} e^{i\mathbf{k}\cdot\mathbf{T}} \phi_{\mu}(\mathbf{r}-\mathbf{T}) \quad (4)$$

and the coefficients are

$$c_{\mu i}^{\mathbf{k}} = \langle \phi_{\mu} | \psi_{i\mathbf{k}} \rangle. \quad (5)$$

Since in present work $|\phi_n\rangle$ is an orthogonal LMTO basis set orbital (in other words n in $|\phi_n\rangle$ corresponds to the particular qlm combination), then $\langle \psi_{i\mathbf{k}} | \phi_n \rangle = c_{ni}^{\mathbf{k}*}$. Hence

$$|\tilde{W}_{n\mathbf{k}}\rangle = \sum_{i=N_1}^{N_2} |\psi_{i\mathbf{k}}\rangle c_{ni}^{\mathbf{k}*} = \sum_{i=N_1}^{N_2} \sum_{\mu} c_{\mu i}^{\mathbf{k}} c_{ni}^{\mathbf{k}*} |\phi_{\mu}^{\mathbf{k}}\rangle. \quad (6)$$

In order to orthonormalize the WFs (6) one needs to calculate the overlap matrix $O_{nn'}(\mathbf{k})$

$$O_{nn'}(\mathbf{k}) \equiv \langle \tilde{W}_{n\mathbf{k}} | \tilde{W}_{n'\mathbf{k}} \rangle = \sum_{i=N_1}^{N_2} c_{ni}^{\mathbf{k}} c_{n'i}^{\mathbf{k}*}, \quad (7)$$

then its inverse square root $S_{nn'}(\mathbf{k})$ is defined as

$$S_{nn'}(\mathbf{k}) \equiv O_{nn'}^{-1/2}(\mathbf{k}). \quad (8)$$

In the derivation of Eq. (7) the orthogonality of Bloch states $\langle \psi_{n\mathbf{k}} | \psi_{n'\mathbf{k}} \rangle = \delta_{nn'}$ was used.

From Eqs. (6) and (8), the orthonormalized WFs in \mathbf{k} space $|W_{n\mathbf{k}}\rangle$ can be obtained as

$$|W_{n\mathbf{k}}\rangle = \sum_{n'} S_{nn'}(\mathbf{k}) |\tilde{W}_{n'\mathbf{k}}\rangle = \sum_{i=N_1}^{N_2} |\psi_{i\mathbf{k}}\rangle c_{ni}^{\mathbf{k}*},$$

$$c_{ni}^{\mathbf{k}*} \equiv \langle \psi_{i\mathbf{k}} | W_{n\mathbf{k}} \rangle = \sum_{n'} S_{nn'}(\mathbf{k}) c_{n'i}^{\mathbf{k}*}.$$

Then the matrix element of the Hamiltonian \hat{H}^{WF} in reciprocal space is

$$H_{nn'}^{\text{WF}}(\mathbf{k}) = \langle W_{n\mathbf{k}} | \left(\frac{1}{N} \sum_{\mathbf{k}'} \sum_{i=N_1}^{N_2} |\psi_{i\mathbf{k}'}\rangle \epsilon_i(\mathbf{k}') \langle \psi_{i\mathbf{k}'} | \right) | W_{n'\mathbf{k}} \rangle$$

$$= \sum_{i=N_1}^{N_2} c_{ni}^{\mathbf{k}} c_{n'i}^{\mathbf{k}*} \epsilon_i(\mathbf{k}). \quad (9)$$

Hamiltonian matrix element in real space is

$$H_{nn'}^{\text{WF}}(\mathbf{T}) = \langle W_n^0 | \hat{H} | W_{n'}^{\mathbf{T}} \rangle = \frac{1}{N} \sum_{\mathbf{k}} \sum_{i=N_1}^{N_2} c_{ni}^{\mathbf{k}} c_{n'i}^{\mathbf{k}*} \epsilon_i(\mathbf{k}) e^{-i\mathbf{k}\cdot\mathbf{T}},$$

here atom n' is shifted from its position in the primary unit cell by a translation vector \mathbf{T} . For more detailed description of this procedure see Ref. 36.

B. LDA band structure, hopping and Coulomb parameters for p - and n -type cuprates

Basically all cuprates have one or more CuO_2 planes in their structure, which are separated by layers of other elements (Ba, Nd, La, ...). They provide the carriers in CuO_2 plane and according to the type of carriers all cuprates can be

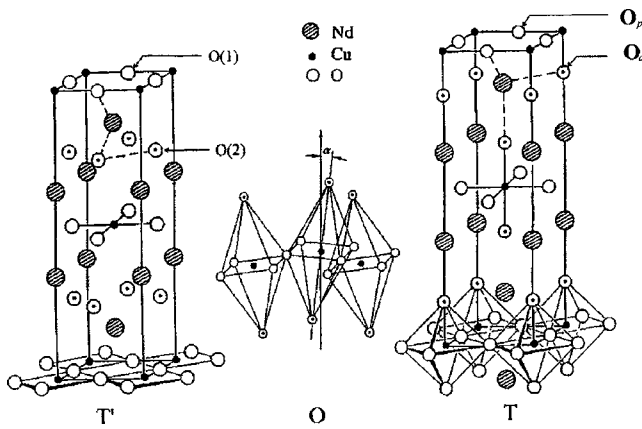


FIG. 1. T' -structure of tetragonal Nd_2CuO_4 on the left, and T structure of the HTT phase (tetragonal, K_2NiF_4 type) of the La_2CuO_4 on the right. Orthorhombic distortions and rotation of the CuO_6 octahedra in the LTO phase of the La_2CuO_4 are schematically shown in the middle. The figure is taken from Ref. 37.

divided into two classes: p type and n type. In the present paper we deal with the simplest representatives of these two classes $\text{La}_{2-x}\text{Sr}_x\text{CuO}_4$ (LSCO) and $\text{Nd}_{2-x}\text{Ce}_x\text{CuO}_4$ (NCCO), correspondingly.

La_2CuO_4 at the low temperature and zero doping has the orthorhombic structure (LTO) with the space group $Bmab$.³⁸ The lattice parameters and atomic coordinates at 10 K were taken from Ref. 38 to be $a=5.3346$, $b=5.4148$, and $c=13.1172$ Å, La (0, -0.0083, 0.3616), Cu (0,0,0), O_p (0.25, 0.25, -0.0084), O_a (0, 0.0404, 0.1837). Here and below O_p denotes in-plane oxygen ions and O_a , apical oxygen ions. In comparison with high-temperature tetragonal structure (HTT) orthorhombic La_2CuO_4 have two formula units per unit cell and the CuO_6 octahedra are rotated cooperatively about the [110] axis (see Fig. 1). As a result O_p ions are slightly moved off the Cu plane and four in-plane La- O_a bond lengths are unequal.

Nd_2CuO_4 at the room temperature and zero doping has the tetragonal structure with the space group $I4/mmm$ (Ref. 39) also called T' -structure (Fig. 1). The lattice parameters are $a=b=3.94362$, $c=12.1584$ Å.³⁹ Cu ions at the $2a$ site (0, 0, 0) are surrounded by four oxygen ions O1 which oc-

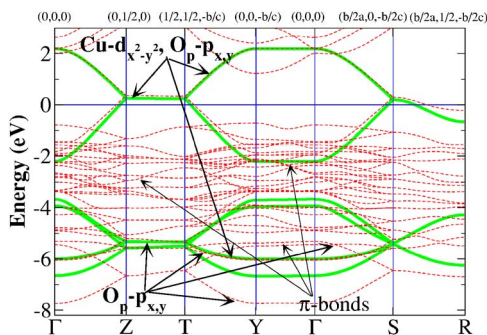


FIG. 2. (Color online) Comparison of the band structure of La_2CuO_4 from LDA calculation (dotted lines) and from projection on the $\text{Cu-}d_{x^2-y^2}$ and O_p - p_x , O_p - p_y set of orbitals (bold solid lines). Fermi level corresponds to zero energy.

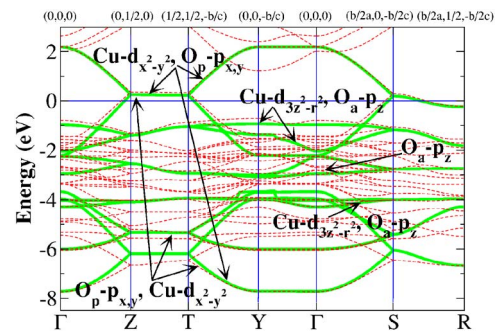


FIG. 3. (Color online) The same as in Fig. 2 but projection is done on the $\text{Cu-}d_{x^2-y^2}$, $\text{Cu-}d_{3z^2-r^2}$ and O_p - p_x , O_p - p_y , O_a - p_z set of orbitals.

cupy $4c$ position (0, 1/2, 0). The Nd at the $4e$ site (0, 0, 0.35112) have eight nearest oxygen ions neighbors O2 at $4d$ position (0, 1/2, 1/4).³⁹ One can imagine body-centered T' structure as the HTT structure of La_2CuO_4 but with two oxygen atoms moved from apices of each octahedron to the face of the cell at the midpoints between two oxygen atoms on the neighboring CuO_2 planes (Fig. 1). In other words Nd_2CuO_4 in T' -structure has no apical oxygens around Cu ion.

LDA band calculation for La_2CuO_4 and Nd_2CuO_4 was done within LMTO method³⁵ using atomic sphere approximation in tight-binding approach⁴⁰ (TB-LMTO-ASA). In the case of Nd_2CuO_4 Nd- $4f$ states were treated as pseudocore states.

The LDA band structure of both compounds along the high-symmetry lines in the Brillouin zone is shown in Figs. 2–5 by dotted lines. The coordinates of high-symmetry points in BZ are given on top of each picture. The complex of bands in the energy range (-8, 2.5) eV consists primarily of Cu- $3d$ and O- $2p$ states. The total bandwidths amount 10 eV for La cuprate and 7 eV for Nd cuprate. Contribution of Cu- $3d$ and O- $2p$ orbitals to the different bands is displayed by arrows.

One can see that the band crossing E_F have character of $\text{Cu-}d_{x^2-y^2}$ and O_p - $p_{x,y}$ for La_2CuO_4 and $\text{Cu-}d_{x^2-y^2}$, $O1$ - $p_{x,y}$ in the case of Nd_2CuO_4 . It corresponds to antibonding $pd\sigma$ orbital. So for hoppings calculation the projection on

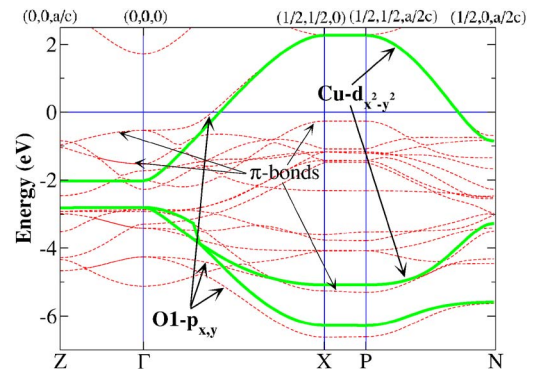


FIG. 4. (Color online) Comparison of the band structure of Nd_2CuO_4 from LDA calculation (dotted lines) and from projection on the $\text{Cu-}d_{x^2-y^2}$, $O1$ - p_x , and $O1$ - p_y set of orbitals (bold solid lines). Fermi level corresponds to zero energy.

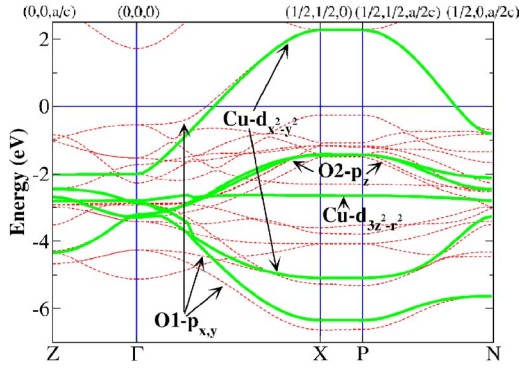


FIG. 5. (Color online) The same as in Fig. 4 but projection is done on the $\text{Cu-}d_{x^2-y^2}$, $\text{Cu-}d_{3z^2-r^2}$ and $\text{O1-}p_x$, $\text{O1-}p_y$, $\text{O2-}p_z$ set of orbitals.

$\text{Cu-}d_{x^2-y^2}$, O_p - p_x , O_p - p_y orbitals for La cuprate and $\text{Cu-}d_{x^2-y^2}$, $\text{O1-}p_x$, $\text{O1-}p_y$ orbitals for Nd cuprate was done. Such set of orbitals corresponds to the three-band p - d model. The bands obtained by the projection procedure described in Sec. II A are shown by solid lines in Figs. 2 and 4. It is clearly seen that in the case of La_2CuO_4 the 3-band model did not reproduce the band crossing E_F properly (Fig. 2, SR direction).

Since the three-band p - d model did not provide proper description of the LDA bands around Fermi level the projection on more complex set of trial orbitals for both compounds was done. The resulting bands are plotted by solid lines in Figs. 3 and 5. Corresponding multiband p - d model contains $\text{Cu-}d_{x^2-y^2}$, $\text{Cu-}d_{3z^2-r^2}$, O_p - p_x , O_p - p_y , O_a - p_z states for La_2CuO_4 and $\text{Cu-}d_{x^2-y^2}$, $\text{Cu-}d_{3z^2-r^2}$, $\text{O1-}p_x$, $\text{O1-}p_y$, $\text{O2-}p_z$ states for Nd_2CuO_4 . The energy range for projection was $(-8.4, 2.5)$ eV and $(-8, 2)$ eV for the case of La cuprate and Nd cuprate correspondingly. The main effect of taking into account $\text{Cu-}d_{3z^2-r^2}$ and O_a - p_z states for La_2CuO_4 is the proper description of the band structure (in comparison with LDA calculation) at the energies up to 2 eV below Fermi level. From Figs. 4 and 5 one can see that in case of Nd_2CuO_4 both sets of trial orbitals properly describe the LDA band crossing the Fermi level which has $\text{Cu-}d_{x^2-y^2}$ symmetry. At the same time its bonding part does not agree well with the LDA bands since projection did not include all Cu- d and O- p orbitals.

The resulting hopping parameters and energy of particular orbitals for two sets of trial orbitals are presented in Tables I and II. The second column contains the connecting vector \mathbf{T} between two sites. It is clearly seen that hoppings decay quite rapidly with distance between ions.

For the multiband p - d model the values of Coulomb parameters are also required. For Cu in La_2CuO_4 they were obtained in constrained LDA supercell calculations⁴¹ to be $U=10$ eV and $J=1$ eV.⁴² For the Nd_2CuO_4 we will use the same values of these parameters.

III. GTB METHOD OVERVIEW

As the starting model that reflects chemical structure of the cuprates it is convenient to use the three-band p - d

TABLE I. Hopping parameters and single electron energies for orthorhombic La_2CuO_4 obtained in WF projection procedure for different sets of trial orbitals (all values in eV). Here x^2 , z^2 , p_x , p_y , p_z denote $\text{Cu-}d_{x^2-y^2}$, $\text{Cu-}d_{3z^2-r^2}$, O_p - p_x , O_p - p_y , O_a - p_z orbitals, correspondingly. The third and fourth columns correspond to bases of the three-band and the multiband p - d models, respectively.

Hopping	Connecting vector	$\text{Cu-}x^2$ $\text{O } p_x, p_y$	$\text{Cu-}x^2, z^2$ $\text{O-}p_x, p_y, p_z$
		$E_{x^2}=-1.849$	$E_{x^2}=-1.849$
		$E_{p_x}=-2.767$	$E_{z^2}=-2.074$
		$E_{p_y}=-2.767$	$E_{p_x}=-2.806$
			$E_{p_y}=-2.806$
			$E_{p_z}=-1.676$
$t(x^2, x^2)$	$(-0.493, -0.5)$	-0.188	-0.188
$t'(x^2, x^2)$	$(-0.985, 0.0)$	0.001	0.002
$t(z^2, z^2)$	$(-0.493, -0.5)$		0.054
$t'(z^2, z^2)$	$(-0.985, 0.0)$		-0.001
$t(x^2, p_x)$	$(0.246, 0.25, -0.02)$	1.357	1.355
$t'(x^2, p_x)$	$(-0.739, 0.25, -0.02)$	-0.022	-0.020
$t(z^2, p_x)$	$(0.246, 0.25, -0.02)$		-0.556
$t'(z^2, p_x)$	$(-0.739, 0.25, -0.02)$		-0.028
$t(z^2, p_z)$	$(0, 0.04, 0.445)$		0.773
$t'(z^2, p_z)$	$(-0.493, -0.46, -0.445)$		-0.011
$t(p_x, p_y)$	$(0.493, 0.0)$	-0.841	-0.858
$t'(p_x, p_y)$	$(0, 0.5, 0.041)$	0.775	0.793
$t''(p_x, p_y)$	$(0.985, 0.5, 0.041)$	-0.001	-0.001
$t(p_x, p_z)$	$(-0.246, -0.21, 0.465)$		-0.391
$t'(p_x, p_z)$	$(0.246, 0.29, -0.425)$		-0.377
$t''(p_x, p_z)$	$(0.246, -0.21, -0.746)$		0.018

model^{23,24} or the multiband p - d model.⁴³ While the first one is simpler it lacks for some significant features, namely, importance of d_{z^2} orbitals on copper and p_z orbitals on apical oxygen. Nonzero occupancy of d_{z^2} orbitals was pointed out in XAS and EELS experiments which shows 2–10 % occupancy of d_{z^2} orbitals^{44,45} and 15% doping dependent occupancy of p_z orbitals⁴⁶ in all hole doped high- T_c compounds. Henceforth the multiband p - d model will be used.

Let us consider the Hamiltonian with the following general structure:

$$H = \sum_{f,\lambda,\sigma} (\epsilon_\lambda - \mu) n_{f\lambda\sigma} + \sum_{f \neq g} \sum_{\lambda,\lambda',\sigma} T_{fg}^{\lambda\lambda'} c_{f\lambda\sigma}^\dagger c_{g\lambda'\sigma} + \frac{1}{2} \sum_{f,g,\lambda,\lambda'} \sum_{\sigma_1,2,3,4} V_{fg}^{\lambda\lambda'} c_{f\lambda\sigma_1}^\dagger c_{f\lambda\sigma_3}^\dagger c_{g\lambda'\sigma_2}^\dagger c_{g\lambda'\sigma_4}, \quad (10)$$

where $c_{f\lambda\sigma}$ is the annihilation operator in Wannier representation of the hole at site f at orbital λ with spin σ , $n_{f\lambda\sigma} = c_{f\lambda\sigma}^\dagger c_{f\lambda\sigma}$.

TABLE II. Hopping parameters and single electron energies for Nd_2CuO_4 obtained in WF projection procedure for different sets of trial orbitals (all values in eV). Here x^2 , z^2 , p_x , p_y , p_z denote $\text{Cu}-d_{x^2-y^2}$, $\text{Cu}-d_{3z^2-r^2}$, $\text{O}1-p_x$, $\text{O}1-p_y$, $\text{O}2-p_z$ orbitals, correspondingly. The third and fourth columns correspond to bases of the three-band and the multiband $p-d$ models, respectively.

Hopping	Connecting vector	Cu- x^2 , O p_x, p_y	Cu- x^2, z^2 , O- p_x, p_y, p_z
		$E_{x^2}=-1.989$	$E_{x^2}=-1.991$
		$E_{p_x}=-3.409$	$E_{z^2}=-2.778$
		$E_{p_z}=-3.409$	$E_{p_x}=-3.368$
			$E_{p_z}=-2.30$
$t(x^2, x^2)$	(1, 0)	0.01	0.01
$t'(x^2, x^2)$	(1, 1)	-0.00	-0.00
$t(z^2, z^2)$	(1, 0)		0.01
$t'(z^2, z^2)$	(1, 1)		0.00
$t(x^2, p_x)$	(0.5, 0)	1.18	1.18
$t'(x^2, p_x)$	(0.5, 1)	-0.06	-0.06
$t'(x^2, p_x)$	(1.5, 0)	0.04	0.04
$t'''(x^2, p_x)$	(1.5, 1)	0.00	0.00
$t(z^2, p_x)$	(0.5, 0)		-0.29
$t'(z^2, p_x)$	(0.5, 1)		0.01
$t(z^2, p_z)$	(0, 0.5, 0.771)		0.10
$t'(z^2, p_z)$	(1, 0.5, 0.771)		0.02
$t(p_x, p_y)$	(0.5, 0.5)	0.69	0.67
$t'(p_x, p_y)$	(1.5, 0.5)	0.00	0.00
$t(p_x, p_z)$	(0.5, 0.5, 0.771)		0.02
$t'(p_x, p_z)$	(0.5, -0.5, 0.771)		0.02

In the particular case of cuprates and corresponding multiband $p-d$ model, f runs through copper and oxygen sites, index λ run through $d_{x^2-y^2} \equiv d_{x^2}$ and $d_{3z^2-r^2} \equiv d_{z^2}$ orbitals on copper, p_x and p_y atomic orbitals on the O_p -oxygen sites and p_z orbital on the apical O_a oxygen; ϵ_λ -single-electron energy of the atomic orbital λ . $T_{fg}^{\lambda\lambda'}$ includes matrix elements of hoppings between copper and oxygen (t_{pd} for hopping $d_{x^2} \leftrightarrow p_x, p_y$; $t_{pd}/\sqrt{3}$ for $d_{z^2} \leftrightarrow p_x, p_y$; t'_{pd} for $d_{z^2} \leftrightarrow p_z$) and between oxygen and oxygen (t_{pp} for hopping $p_x \leftrightarrow p_y$; t'_{pp} for hopping $p_x, p_y \leftrightarrow p_z$). The Coulomb matrix elements $V_{fg}^{\lambda\lambda'}$ include intra-atomic Hubbard repulsions of two holes with opposite spins on one copper and oxygen orbital (U_d, U_p), between different orbitals of copper and oxygen (V_d, V_p), Hund exchange on copper and oxygen (J_d, J_p) and the nearest-neighbor copper-oxygen Coulomb repulsion V_{pd} .

GTB method^{22,28,29} consist of exact diagonalization of intracell part of the multiband Hamiltonian (10) and perturbative account of the intercell part. For $\text{La}_{2-x}\text{Sr}_x\text{CuO}_4$ and $\text{Nd}_{2-x}\text{Ce}_x\text{CuO}_4$ the unit cells are CuO_6 and CuO_4 clusters, respectively, and a problem of nonorthogonality of the molecular orbitals of adjacent cells is solved by an explicit fashion using the diagonalization in \mathbf{k} space.⁴⁷ In a new symmet-

ric basis the intracell part of the total Hamiltonian is diagonalized, allowing us to classify all possible effective quasiparticle excitations in CuO_2 -plane according to a symmetry. To describe this process the Hubbard X operators⁴⁸ $X_f^m \leftrightarrow X_f^{p,q} \equiv |p\rangle\langle q|$ are introduced. Index $m \leftrightarrow (p, q)$ enumerates quasiparticle with energy $\omega_m = \epsilon_p(N+1) - \epsilon_q(N)$, where ϵ_p is the p th energy level of the N -electron system. There is a correspondence between Hubbard operators and single-electron creation and annihilation operators

$$c_{f\lambda\sigma} = \sum_m \gamma_{\lambda\sigma}(m) X_f^m, \quad (11)$$

where $\gamma_{\lambda\sigma}(m)$ determines the partial weight of a quasiparticle m with spin σ and orbital index λ . Using this correspondence we rewrite the Hamiltonian (10)

$$H = \sum_{f,p} (\epsilon_p - N\mu) X_f^{p,p} + \sum_{f \neq g} \sum_{m,m'} t_{fg}^{mm'} X_f^{m\dagger} X_g^{m'}. \quad (12)$$

This Hamiltonian, actually, has the form of the multiband Hubbard model.

Diagonalization of the Hamiltonian (10) mentioned above gives energies ϵ_p and the basis of Hubbard operators X_f^m . Values of the hoppings

$$t_{fg}^{mm'} = \sum_{\sigma,\lambda,\lambda'} T_{fg}^{\lambda\lambda'} \gamma_{\lambda\sigma}^*(m) \gamma_{\lambda'\sigma}(m'), \quad (13)$$

are calculated straightforwardly using the exact diagonalization of the intracell part of the Hamiltonian (10).

In the Hamiltonian (12) the intercell hoppings $t_{fg}^{mm'}$ are treated by the perturbation theory over $t/U \ll 1$. In the Mott-Hubbard insulators far from the Mott transition this is a good small parameter. For cuprates, instead of large $t_{pd}=1$ eV the intercluster hoppings are strongly decreased and are less than 0.5 eV [see Eq. (15) and Tables IV and V below], while the effective U is large and given by the value of the charge-transfer gap $E_{ct} \approx 2$ eV.

Again, in the particular case of the multiband $p-d$ model, the essentials for cuprates multielectron configurations are $d^{10}p^6$ (vacuum state $|0\rangle$ in a hole representation), single-hole configurations d^9p^6 , $d^{10}p^5$, and two-hole configurations d^8p^6 , d^9p^5 , $d^{10}p^4$, $d^{10}p^5p^5$. In the single-hole sector of the Hilbert space the b_{1g} molecular orbital, which we will denote later as $|\sigma\rangle = \{|\uparrow\rangle, |\downarrow\rangle\}$, has the minimal energy. In the two-hole sector the lowest energy states are singlet state $|S\rangle$ with ${}^1A_{1g}$ symmetry, that includes Zhang-Rice singlet among other local singlets, and triplet states $|T\rangle = |TM\rangle$ ($M = +1, 0, -1$) with ${}^3B_{1g}$ symmetry.^{28,29,47} All these states form the basis of the Hamiltonian (12), and they are shown together with quasiparticle excitations between them in Fig. 6.

In this basis relations (11) between annihilation-creation operators $c_{f\lambda\sigma}$ and Hubbard X operators X_f^m are

$$c_{fd_{z^2}\sigma} = u X_f^{0,\sigma} + 2\sigma \gamma_x X_f^{\bar{\sigma},S},$$

$$c_{fp_{b\sigma}} = v X_f^{0,\sigma} + 2\sigma \gamma_b X_f^{\bar{\sigma},S},$$

$$c_{fp_{a\sigma}} = \gamma_a (\sigma \sqrt{2} X_f^{\bar{\sigma},T0} - X_f^{\sigma,T2\sigma}),$$

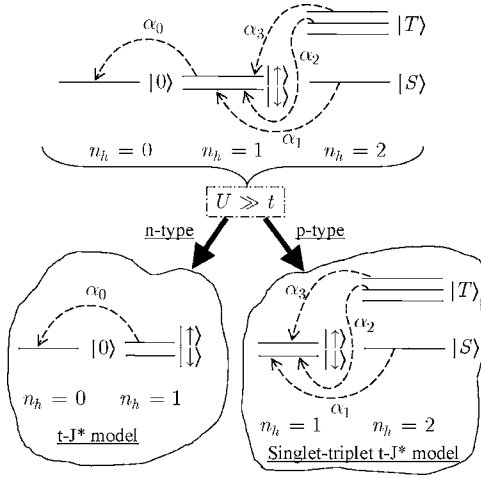


FIG. 6. Schematic picture of states and quasiparticle excitations between them in Hubbard-type model (12). Here n_h stands for number of holes, α_i numerates Fermi-type quasiparticles, states $|0\rangle$, $|\sigma\rangle$, $|S\rangle$, $|T\rangle$ represents basis of the Hamiltonian (12). Also, bases of effective models are shown.

$$c_{fd_2\sigma} = \gamma_z(\sigma\sqrt{2}X_f^{\bar{\sigma},T0} - X_f^{\sigma,T2\sigma}),$$

$$c_{fp_2\sigma} = \gamma_p(\sigma\sqrt{2}X_f^{\bar{\sigma},T0} - X_f^{\sigma,T2\sigma}),$$

and the explicit form of the Hamiltonian (12) is given by

$$\begin{aligned} H_{pd} = & \sum_f \left[\varepsilon_1 \sum_{\sigma} X_f^{\sigma,\sigma} + \varepsilon_{2S} X_f^{S,S} + \varepsilon_{2T} \sum_M X_f^{TM,TM} \right] \\ & + \sum_{f \neq g, \sigma} [t_{fg}^{00} X_f^{\sigma,0} X_g^{0,\sigma} + t_{fg}^{SS} X_f^{S,\bar{\sigma}} X_g^{\bar{\sigma},S} + 2\sigma t_{fg}^{0S} (X_f^{\sigma,0} X_g^{\bar{\sigma},S} \\ & + \text{H.c.}) + t_{fg}^{ST} \{ (\sigma\sqrt{2}X_f^{T0,\bar{\sigma}} - X_f^{T2\sigma,\sigma}) (vX_g^{0,\sigma} + 2\sigma\gamma_b X_g^{\bar{\sigma},S}) \\ & + \text{H.c.} \} + t_{fg}^{TT} (\sigma\sqrt{2}X_f^{T0,\bar{\sigma}} - X_f^{T2\sigma,\sigma}) (\sigma\sqrt{2}X_g^{\bar{\sigma},T0} - X_g^{\sigma,T2\sigma})]. \end{aligned} \quad (14)$$

Here $\bar{\sigma} \equiv -\sigma$. The relation between effective hoppings (13) in this Hamiltonian and microscopic parameters of the multi-band p - d model is as follows:^{49,50}

$$\begin{aligned} t_{fg}^{00} &= -2t_{pd}\mu_{fg}2uv - 2t_{pp}v_{fg}v^2, \\ t_{fg}^{SS} &= -2t_{pd}\mu_{fg}^2\gamma_x\gamma_b - 2t_{pp}v_{fg}\gamma_b^2, \\ t_{fg}^{0S} &= -2t_{pd}\mu_{fg}(v\gamma_x + u\gamma_b) - 2t_{pp}v_{fg}v\gamma_b, \\ t_{fg}^{TT} &= \frac{2t_{pd}}{\sqrt{3}}\lambda_{fg}2\gamma_a\gamma_z + 2t_{pp}v_{fg}\gamma_a^2 - 2t'_{pp}\lambda_{fg}2\gamma_p\gamma_a, \\ t_{fg}^{ST} &= \frac{2t_{pd}}{\sqrt{3}}\xi_{fg}\gamma_z + 2t_{pp}X_{fg}\gamma_a - 2t'_{pp}\xi_{fg}\gamma_p. \end{aligned} \quad (15)$$

The factors μ , v , λ , ξ , χ are the coefficients of Wannier transformation made in the GTB method and u , v , γ_x , γ_b , γ_a , γ_p , γ_z are the matrix elements of annihilation-creation operators in the Hubbard X -operator representation.²⁸

TABLE III. Hopping parameters and single-electron energies of holes obtained by fitting GTB band structure to experimental data and in the *ab initio* calculations for p - and n -type cuprates (all values in eV).

	p -type		n -type	
	fitted	<i>ab initio</i>	fitted	<i>ab initio</i>
$\varepsilon_{d_x^2}$	0	0	0	0
ε_{p_x}	1.5	0.91	1.4	1.38
$\varepsilon_{d_z^2}$	0.2	0.14	0.5	0.79
ε_{p_z}	0.45	-0.26	0.45	0.31
t_{pd}	1	1	1	1
t_{pp}	0.46	0.63	0.56	0.57
t'_{pd}	0.58	0.57	0	0.08
t'_{pp}	0.42	0.29	0.1	0.02

Calculations^{28,29} of the quasiparticle dispersion and spectral intensities in the framework of the multiband p - d model by the GTB method are in very good agreement with the ARPES data on insulating compound $\text{Sr}_2\text{CuO}_2\text{Cl}_2$.^{51,52} Other significant results of this method are as follows.^{53,54}

(i) Pinning of Fermi level in LSCO at low concentrations was obtained in agreement with experiments.^{55,56} This pinning appears due to the in-gap state, spectral weight of this state is proportional to doping concentration x and when Fermi level comes to this in-gap band then Fermi level “pins” there. The localized in-gap state exists in NCCO also for the same reason as in LSCO, but its energy is determined by the extremum of the band at $(\pi/2, \pi/2)$ point and it appears to be above the bottom of the conductivity band. Thus, the first doped electron goes into the band state at the $(\pi, 0)$ and the chemical potential μ for the very small concentration merges into the band. At higher x it meets the in-gap state with a pinning at $0.08 < x < 0.18$ and then μ again moves into the band. The dependence $\mu(x)$ for NCCO is quite asymmetrical to the LSCO and also agrees with experimental data.⁵⁶

(ii) The experimentally observed⁵⁷ evolution of Fermi surface with doping from hole-type [centered at (π, π)] in the underdoped region to electron-type [centered at $(0, 0)$] in the overdoped region is qualitatively reproduced.

(iii) A pseudogap feature for LSCO is obtained as a lowering of density of states between the in-gap state and the states at the top of the valence band.

In all these calculations the set of the microscopic model parameters, obtained by fitting to experimental ARPES data,^{51,58} was used. Hoppings and single-electron energies are listed in Table III, values of Coulomb parameters are as follows:

$$U_d = V_d = 9, \quad U_p = V_p = 4,$$

$$J_d = 1, \quad J_p = 0, \quad V_{pd} = 1.5. \quad (16)$$

All results above were obtained by treating the intercell hopping in the Hubbard-I approximation.⁵ But the GTB

method is not restricted to such a crude approximation. The Fourier transform of the two-time retarded Green function in energy representation can be rewritten in terms of matrix Green function $D_{k\sigma}^{mn}(E) = \langle\langle X_{k\sigma}^m | X_{k\sigma}^{n\dagger} \rangle\rangle_E$:

$$\langle\langle c_{k\lambda\sigma} | c_{k\lambda\sigma}^\dagger \rangle\rangle_E = \sum_{m,m'} \gamma_{\lambda\sigma}(m) \gamma_{\lambda\sigma}^*(m') D_{k\sigma}^{mm'}(E).$$

The diagram technique for Hubbard X operators is developed^{59,60} and the generalized Dyson equation⁶¹ reads

$$\hat{D}_{k\sigma}(E) = \{[\hat{G}_{k\sigma}^{(0)}(E)]^{-1} + \hat{\Sigma}_{k\sigma}(E)\}^{-1} \hat{P}_{k\sigma}(E). \quad (17)$$

Here, $\hat{\Sigma}_{k\sigma}(E)$ and $\hat{P}_{k\sigma}(E)$ are the self-energy and the strength operators, respectively. The presence of the strength operator is due to the redistribution of the spectral weight that is an intrinsic feature of SCES. First time it was introduced in the spin diagram technique and called ‘‘a strength operator’’⁶² because the value of $\hat{P}_{k\sigma}(E)$ determines an oscillator strength of excitations. It is also should be stressed that $\hat{\Sigma}_{k\sigma}(E)$ in Eq. (17) is the self-energy in X -operator representation and therefore it is different from the self-energy entering Dyson equation for the Green function $\langle\langle c_{k\lambda\sigma} | c_{k\lambda\sigma}^\dagger \rangle\rangle_E$. The Green function $\hat{G}_{k\sigma}^{(0)}(E)$ is defined by the formula

$$[\hat{G}_{k\sigma}^{(0)}(E)]^{-1} = \hat{G}_0^{-1}(E) - \hat{P}_{k\sigma}(E) \hat{t}_{k\sigma}, \quad (18)$$

where $\hat{G}_0^{-1}(E)$ is the free propagator and $\hat{t}_{k\sigma}$ is the interaction matrix element [for the Hubbard model, $t_{k\sigma}^{mm'} = \gamma_{\sigma}(m) \gamma_{\sigma}^*(m') t_k$, and $G_{\sigma}^{mm'}(E) = \delta_{mm'} / (E - \varepsilon_1)$].

In the Hubbard-I approximation at $U \gg W$ the self-energy $\hat{\Sigma}_{k\sigma}(E)$ is equal to zero and the strength operator $\hat{P}_{k\sigma}^{mn}(E)$ is replaced by $\hat{P}_{k\sigma}^{mn}(E) \rightarrow \hat{P}_{\sigma}^{mn} = \delta_{mn} F_{\sigma}^m$, where $F_{\sigma}^m = \langle X_f^{p,p} \rangle + \langle X_f^{q,q} \rangle$ is the occupation factor. So, in this approximation the following equation is derived from Eq. (17):

$$\hat{D}_{k\sigma}^{(0)} = \{\hat{G}_0^{-1}(E) - \hat{P}_{\sigma} \hat{t}_{k\sigma}\}^{-1} \hat{P}_{\sigma}. \quad (19)$$

Using diagram technique for the X operators it is possible to find solution in the GTB method beyond the Hubbard-I approximation. But such discussion is far from the scope of this paper’s goals.

It should be stressed that the GTB bands are not free electron bands of the conventional band structure, these are the quasiparticle bands with the number of states in each particular band depending on the occupation number of the initial and final multielectron configurations, and thus on the electron occupation. Bands with zero spectral weight or spectral weight proportional to doping value x appear in the GTB approach.

IV. LDA+GTB METHOD: RESULTS AND DISCUSSION

In this section we will describe the LDA+GTB method itself and some results of this approach. In the LDA+GTB scheme all parameters of the multiband model are calculated within the *ab initio* LDA (by Wannier function projection technique, see Sec. II A) and constrained LDA method.⁴¹ Analysis of the LDA band structure gives the minimal model

that should be used to describe the physics of system under consideration. Although LDA calculation does not give correct description of the SCES band structure, it gives *ab initio* parameters and reduced number of essential orbitals or the ‘‘minimal reliable model.’’ Then the effects of strong electron correlations in the framework of this model with *ab initio* calculated parameters are explicitly taken into account within the GTB method, and the quasiparticle band structure is derived.

In Sec. II the *ab initio* calculations for undoped La_2CuO_4 and Nd_2CuO_4 are presented. One can see that in the three-band model (Figs. 2 and 4) it is possible to describe the bands crossing the Fermi level but not the lower lying excitations within 4 eV. The main effect of taking into account $\text{Cu-}d_{3z^2-r^2}$ and $\text{O}_a\text{-}p_z$ states for La_2CuO_4 system is the proper description of the band structure (in comparison with LDA calculation) at the energies up to 4 eV below Fermi level (see Fig. 3). Of course, the *ab initio* LDA band structure is not correct in undoped cuprates, but it gives an indication of what orbitals should be included in more appropriate calculations. Therefore if one needs to describe quantitatively the low-energy excitations of $\text{La}_{2-x}\text{Sr}_x\text{CuO}_4$, the $\text{Cu-}d_{3z^2-r^2}$ and $\text{O}_a\text{-}p_z$ orbitals should be taken into account and the reliable minimal model is the multiband p - d model. In Nd_2CuO_4 the $\text{Cu-}d_{3z^2-r^2}$ and $\text{O}_2\text{-}p_z$ states do not contribute significantly to the band structure (compare Figs. 4 and 5) and the minimal model is the three-band p - d model. There is the physical reason why both $d_{x^2-y^2}$ and $d_{3z^2-r^2}$ states are necessary in the basis for the low energy description of La_2CuO_4 and $d_{3z^2-r^2}$ state is not necessary for Nd_2CuO_4 . In La_2CuO_4 with T structure (see Fig. 1) the tetragonal component of the crystal field is small (≤ 0.5 eV), and so the splitting of the two e_g levels is also small. In Nd_2CuO_4 with T' -structure the apical oxygen is absent, so the tetragonal component of the crystal field is large and is of the same order of magnitude as the cubic component. That is why the splitting of e_g levels is large, and $d_{3z^2-r^2}$ hole has rather high energy and is not important in the low excitation energy calculations for Nd_2CuO_4 . Nevertheless to treat p - and n -type cuprates on equal footing later we will use the same multiband p - d model for both LSCO and NCCO with different material-dependent parameters. Hopping parameters decay rapidly with distance (see Tables I and II) so in GTB calculation we will use only nearest copper-oxygen and oxygen-oxygen hoppings which are listed in Table III.

In Refs. 63 and 64 *ab initio* calculations were done for $\text{YBa}_2\text{Cu}_3\text{O}_7$ and La_2CuO_4 , and single-electron energy $\varepsilon_{p_x} = 0.9$ eV was obtained. This value is very close to the one presented in Table III. But in Refs. 63 and 64 the $\text{Cu-}s$ states were taken into account with energy $\varepsilon_s = -6.5$ eV. Our LDA calculations show that $\text{Cu-}s$ bands contribute to the band structure shown in Figs. 3 and 5 at approximately 7 eV below and at 2 eV above Fermi level. Therefore $\text{Cu-}s$ states do not contribute significantly to the low-energy physics. But these states can contribute to the effective intraplane hopping parameters t' and t'' between the nearest- and next-nearest-neighbor unit cells. In our LDA+GTB method $\text{Cu-}s$ states are neglected. It could be a reason why for La_2CuO_4 our $t'/t = -0.137$ (see Table IV) is less than $t'/t = -0.17$ ob-

TABLE IV. Parameters of the multiband Hubbard model (12) and exchange integral J for LSCO obtained in the framework of the LDA+GTB method (all values in eV). Hoppings giving main contribution to the top of the valence band are shown by bold type.

ρ	t_{ρ}^{00}	t_{ρ}^{SS}	t_{ρ}^{OS}	t_{ρ}^{TT}	t_{ρ}^{ST}	J_{ρ}
(0,1)	0.453	0.679	0.560	0.004	-0.086	0.157
(1,1)	-0.030	-0.093	-0.055	-0.001	0	0.001
(0,2)	0.068	0.112	0.087	0.002	-0.016	0.004
(2,1)	0.003	-0.005	0	0	-0.002	0

tained in Ref. 64, where influence of Cu- s orbital on hoppings was taken into account.

There is a claim that $pd\pi$ -bonds⁶⁵ and nonbonding oxygen states⁶⁶ are very important in low-energy physics of high- T_c cuprates. To discuss this topic let us start with analysis of *ab initio* calculations. Present LDA calculations show that antibonding bands π^* of π bonds (Cu- $d+O-p\pi$, see Figs. 2 and 4) situated slightly below antibonding σ_a^* bands of Cu- $d_{3z^2-r^2}+O_a-p_z$ origin in La_2CuO_4 and slightly above antibonding σ_a^* bands of Cu- $d_{3z^2-r^2}$ origin in Nd_2CuO_4 (see Figs. 3 and 5). GTB calculations²⁸ show that states corresponding to σ_a^* band contributes to the a_{1g} molecular orbital in the single-hole sector of the Hilbert space. This a_{1g} molecular orbital situated above b_{1g} state $|\sigma\rangle=\{|\uparrow\rangle, |\downarrow\rangle\}$ by an energy about 1.2 eV. From the relative position of σ_a^* and π^* bands in LDA calculations we conclude that the energy of molecular orbital corresponding to the π^* band will be situated around energy of a_{1g} state. Therefore, it will be above $|\sigma\rangle$ state by about 1.0–1.4 eV. Also, both states corresponding to π^* and σ_a^* are empty in undoped compound and spectral weight of quasiparticle excitations to or from these states will be zero. Summarizing, π bonds, as well as σ_a^* states, will contribute to the GTB dispersion only upon doping and only in the depth in the valence band below 1 eV from the top. Moreover, since energy difference between triplet $|T\rangle$ and singlet $|S\rangle$ states is about 0.5 eV,²⁸ the contribution from the singlet-triplet excitations will be much more important to the low-energy physics. Although, π bonds could be important for explanation of some optical and electron-energy loss spectroscopy experiments, but in description of low-energy physics of interest they could be neglected. The nonbonding oxygen states contribute to the valence band with energy about 2–3 eV below the top. That is why we will not take π bonds and nonbonding oxygen states in our further consideration.

Now we have an idea what model should be used and *ab initio* microscopic parameters of this model. As described in Sec. III, the GTB method is appropriate method for description of SCES in Mott-Hubbard type insulators and its results are in good agreement with experimental data. Then it is natural to use this method to work with the *ab initio* derived multiband p - d model.

The parameters (15) of the Hamiltonian in the GTB method derived from *ab initio* one are presented in Tables IV and V for p - and n -type cuprates, respectively. Single-electron energies (in eV) and matrix elements of annihilation-creation operators in the X operators representation were calculated for both LSCO

TABLE V. The same as in Table IV, but for NCCO. Hoppings giving main contribution to the bottom of the conductivity band are shown by bold type.

ρ	t_{ρ}^{00}	t_{ρ}^{SS}	t_{ρ}^{OS}	t_{ρ}^{TT}	t_{ρ}^{ST}	J_{ρ}
(0,1)	0.410	0.645	-0.523	0	-0.0052	0.137
(1,1)	-0.013	-0.076	0.035	0	0	0.001
(0,2)	0.058	0.104	-0.078	0	-0.0002	0.003
(2,1)	0.005	-0.002	-0.003	0	-0.0004	0

$$\epsilon_1 = -1.919, \quad \epsilon_{2S} = -2.010, \quad \epsilon_{2T} = -1.300,$$

$$u = -0.707, \quad v = -0.708, \quad \gamma_x = -0.619,$$

$$\gamma_b = -0.987, \quad \gamma_a = -0.032, \quad \gamma_p = -0.962, \quad \gamma_z = -0.237 \quad (20)$$

and NCCO

$$\epsilon_1 = -1.660, \quad \epsilon_{2S} = -1.225, \quad \epsilon_{2T} = -0.264,$$

$$u = -0.756, \quad v = -0.655, \quad \gamma_x = 0.626,$$

$$\gamma_b = 0.984, \quad \gamma_a = -0.008, \quad \gamma_p = 0.997, \quad \gamma_z = 0.037. \quad (21)$$

It is known⁶⁷ that sign of the hoppings in the t - t' - t'' - J model changes during electron-hole transformation of the operators. Therefore, t_{ρ} will have different signs in p - and n -type cuprates. In present paper we do not do electron-hole transformation of the operators, and both t - t' - t'' - J^* and singlet-triplet t - t' - t'' - J^* models are written using hole operators. Because of that there is no difference in signs of the hoppings t_{ρ} for the hole- and electron-doped systems presented in Tables IV and V.

As the next step we calculate the band structure of the undoped antiferromagnetic (AFM) insulating cuprate within the GTB method. Results for both GTB method with fitting parameters and LDA+GTB method with *ab initio* parameters (Table III) are presented in Fig. 7 for La_2CuO_4 and in Fig. 8 for Nd_2CuO_4 .

The GTB band structure obtained for both phenomenological and *ab initio* sets of parameters is almost identical: the valence band, located below 0 eV in figures, and the conductivity band, located above +1.5 eV, divided by the insulator gap of the charge transfer origin $E_{ct} \approx 2$ eV; the undoped La_2CuO_4 and Nd_2CuO_4 are insulators in both antiferromagnetic and paramagnetic states. In-gap states at the top of the valence band and about the bottom of the conductivity band are shown by dashed lines. Their spectral weights and dispersions are proportional to doping x and concentration of magnons.⁶⁸ Therefore, for undoped compounds, in the Hubbard-I approximation used in GTB method, these states are dispersionless with zero spectral weight.

The valence band have bandwidth about 6 eV and consists of a set of very narrow subbands with the highest one at the top of the valence band—the so-called “Zhang-Rice sin-

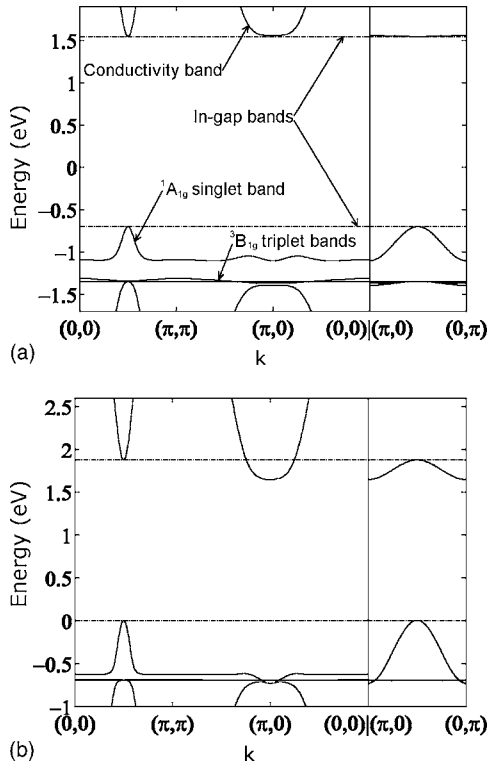


FIG. 7. The AFM band structure of La_2CuO_4 obtained in the GTB method with phenomenological set of parameters (a) and in the LDA+GTB method (b). In the figure (a) bands are labeled; in other GTB band structure figures relative positions of bands are the same.

glet" subband. The dominant spectral weight in the singlet band stems from the oxygen p states, while for the bottom of the empty conductivity band it is from $d_{x^2-y^2}$ states of copper. Both methods give small, less than 0.5 eV, splitting between the $^1A_{1g}$ Zhang-Rice-type singlet band and $^3B_{1g}$ narrow triplet band located below the singlet band (e.g., in Fig. 8 for Nd_2CuO_4 it is located at -1.5 eV). The energy of Cu $-d_{3z^2-r^2}$ orbital plays the dominant role in this splitting in the GTB method. For La_2CuO_4 energy ε_{d_z} is smaller than for Nd_2CuO_4 (see Table III). This results in smaller width of the singlet band for the LSCO compared to the NCCO: about 0.5 eV and 1 eV correspondingly.

However, for La_2CuO_4 minor discrepancies occur in the dispersion of the bottom of the conductivity band near $(\pi, 0)$ point obtained by GTB with phenomenological set of parameters and by LDA+GTB. This leads to the different character of the optical absorption edge in two presented methods. The absorption edge for the LDA+GTB is formed by the indirect transitions in contrast to the GTB method with phenomenological set of parameters, where the momentum of excited quasiparticle is conserved by optical transition at the absorption edge. For Nd_2CuO_4 both GTB method with fitting parameters and LDA+GTB result in the conductivity band minima at the $(\pi, 0)$ point (see Fig. 8). Also, in the LDA+GTB method the triplet band dispersion and the singlet-triplet hybridization are much smaller than in the GTB method with fitting parameters. This happens mainly due to the smaller values of t'_{pp} used in LDA+GTB method, be-

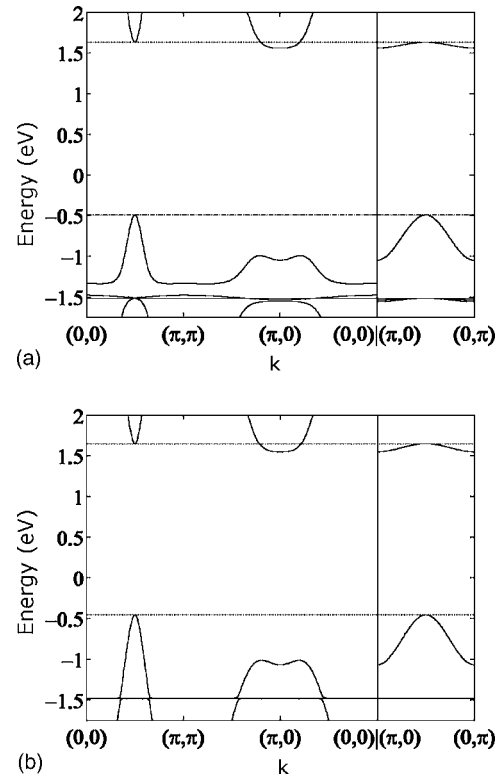


FIG. 8. The AFM band structure of Nd_2CuO_4 obtained in the GTB method with phenomenological set of parameters (left) and in the LDA+GTB method (right).

cause it is this microscopic parameter that gives main numerical contribution [see Eqs. (15), (20), and (21)] to the t'_{fg} and t'_{fg}^{ST} hoppings that determines the triplet band dispersion and the singlet-triplet hybridization, respectively. So, despite some minor discrepancies, both GTB method with phenomenological parameters and LDA+GTB method without free parameters give similar band dispersion.

Next topic that we will discuss in connection to the LDA+GTB method is the value of magnetic moment on copper M_{Cu} . From the neutron diffraction studies of La_2CuO_4 (Ref. 69) and $\text{YBa}_2\text{Cu}_3\text{O}_6$ (Ref. 70) it is known that M_{Cu} is equal to $0.5\mu_B$ where μ_B is Bohr magneton. There are two reasons why M_{Cu} is different from the free atomic value $1.14\mu_B$ in $S=1/2\text{Cu}^{2+}$, namely, zero temperature quantum spin fluctuations and the covalent effect. Since each oxygen has two neighboring coppers belonging to different magnetic sublattices the total moment on oxygen is equal to zero. But due to p - d hybridization the p states of oxygen are partially filled so these orbitals could carry non-zero magnetic moment M_{O} , while total moment on oxygen will be equal to zero. Such space distribution of magnetic moment leads to the difference⁷¹ between experimentally observed antiferromagnetic form factor for La_2CuO_4 and the Heisenberg form-factor of Cu^{2+} . In order to take into account covalent effects and zero quantum fluctuations on equal footing we will write down the expression for M_{Cu} :

$$M_{\text{Cu}} = 2.28\mu_B \langle S^z \rangle u^2, \quad (22)$$

where zero quantum spin fluctuations are contained in $\langle S^z \rangle$ and covalent effects are described by the weight u^2 of the

d^9p^6 configuration. The last quantity is calculated in the framework of the LDA+GTB method and equal to $u^2=0.5$. In Ref. 72 the value $\langle S^z \rangle = 0.3$ was obtained self-consistently in the effective quasi-two-dimensional Heisenberg antiferromagnetic model for typical in La_2CuO_4 ratio 10^{-5} of the interplane and intraplane exchange parameters. Close value of $\langle S^z \rangle = 0.319$ was obtained in Ref. 73 where also the plaquette ring-exchange was considered in Heisenberg Hamiltonian. Using Eq. (22) and above values of u^2 and $\langle S^z \rangle$ we have calculated magnetic moment on copper $M_{\text{Cu}} = 0.4\mu_B$, that is close to the experimentally observed $M_{\text{Cu}} = 0.5\mu_B$.

Summarizing this section, we can conclude that the proposed LDA+GTB scheme works quite well and could be used for quantitative description of the high- T_c cuprates. The LDA+GTB scheme also can be used for wide class of SCESs—cuprates, manganites, and others.

V. EFFECTIVE LOW-ENERGY MODEL

When we are interested in the low-energy physics (such as, e.g., superconductivity) it is useful to reduce the microscopic model to a simpler effective Hamiltonian. For example, for the Hubbard model in the regime of strong correlations the effective model is the t - J^* model (t - J model plus three-center correlated hoppings H_3) obtained by exclusion of the intersubband hoppings perturbatively.^{74–76} Analysis of the three-band model results in the effective Hubbard and the t - J model.^{25,27,77–79}

As the next step we will formulate the effective model for the multiband p - d model. The simplest way to do it is to neglect completely contribution of two-particle triplet state $^3B_{1g}$. Then there will be only one low-energy two-particle state—Zhang-Rice-type singlet $^1A_{1g}$ —and the effective model will be the usual t - J^* model. But in the multiband p - d model the difference $\epsilon_T - \epsilon_S$ between energy of two-particle singlet and two-particle triplet depends strongly on various model parameters, particularly on distance of the apical oxygen from the planar oxygen, energy of the apical oxygen, difference between energy of d_{z^2} orbitals and d_{x^2} orbitals. For the realistic values of model parameters $\epsilon_T - \epsilon_S$ is close to 0.5 eV (Refs. 29 and 47) contrary to the three-band model with this value being about 2 eV. To take into account triplet states we will derive the effective Hamiltonian for multiband p - d model by exclusion of the intersubband hopping between low (LHB) and upper (UHB) Hubbard subbands. These subbands divided by the energy of charge-transfer gap $E_{ct} \approx 2$ eV (similar to U in the Hubbard model) and using perturbation theory, similar to Ref. 75, with small parameter W/U we can derive separate effective models for UHB and LHB. This procedure is schematically shown in Fig. 6. And, as one can see, since the UHB and LHB in initial model (14) are formed by different quasiparticles (namely, α_0 for LHB and $\alpha_1, \alpha_2, \alpha_3$ for UHB in Fig. 6), the effective models will be different for upper (valence band, hole doped) and lower (conductivity band, electron doped) subbands.

We write the Hamiltonian in the form $H = H_0 + H_1$, where the excitations via the charge transfer gap E_{ct} are included in

H_1 . Then we define an operator $H(\epsilon) = H_0 + \epsilon H_1$ and make the unitary transformation $\tilde{H}(\epsilon) = \exp(-i\epsilon\hat{S})H(\epsilon)\exp(i\epsilon\hat{S})$. Vanishing linear in ϵ component of $\tilde{H}(\epsilon)$ gives the equation for matrix \hat{S} : $H_1 + i[H_0, \hat{S}] = 0$. The effective Hamiltonian is obtained in second order in ϵ and at $\epsilon=1$ is given by $\tilde{H} = H_0 + \frac{1}{2}i[H_1, \hat{S}]$. For the multiband p - d model (14) in case of electron doping we obtain the usual t - J^* model describing conductivity band

$$H_{t-J^*} = \sum_{f,\sigma} \epsilon_1 X_f^{\sigma,\sigma} + \sum_{f \neq g,\sigma} t_{fg}^{00} X_f^{\sigma,0} X_g^{0,\sigma} + \sum_{f \neq g \neq m,\sigma} H_3 + \sum_{f \neq g} J_{fg} \left(\vec{S}_f \vec{S}_g - \frac{1}{4} n_f n_g \right), \quad (23)$$

here H_3 contains three-centers interaction terms given by Eq. (A1), \vec{S}_f are spin operators and n_f are number of particles operators. The $J_{fg} = 2(t_{fg}^{0S})^2/E_{ct}$ is the exchange parameter.

For p -type systems the effective Hamiltonian has the form of the singlet-triplet t - J^* model describing valence band

$$H_{\text{eff}} = H_0 + H_t + \sum_{f \neq g \neq m,\sigma} H_{\text{eff}3} + \sum_{f \neq g} J_{fg} \left(\vec{S}_f \vec{S}_g - \frac{1}{4} n_f n_g \right). \quad (24)$$

Three-centers interaction terms $H_{\text{eff}3}$ are given by Eq. (A2). Expressions for H_0 and H_t are as follows:

$$H_0 = \sum_f \left[\epsilon_1 \sum_{\sigma} X_f^{\sigma,\sigma} + \epsilon_{2S} X_f^{S,S} + \epsilon_{2T} \sum_M X_f^{TM, TM} \right],$$

$$H_t = \sum_{f \neq g,\sigma} \{ t_{fg}^{SS} X_f^{S,\bar{\sigma}} X_g^{\bar{\sigma},S} + t_{fg}^{TT} (\sigma \sqrt{2} X_f^{T0,\bar{\sigma}} - X_f^{T2,\sigma}) (\sigma \sqrt{2} X_g^{\bar{\sigma},T0} - X_g^{\sigma,T2\sigma}) + t_{fg}^{ST} 2\sigma \gamma_b [X_f^{S,\bar{\sigma}} (\sigma \sqrt{2} X_g^{\bar{\sigma},T0} - X_g^{\sigma,T2\sigma}) + \text{H.c.}] \}.$$

The resulting Hamiltonian (24) is the two-band generalization of the t - J^* model. Significant feature of effective singlet-triplet model is the asymmetry for n - and p -type systems which is known experimentally. So, we can conclude that for n -type systems the usual t - J^* model takes place while for p -type superconductors with complicated structure on the top of the valence band the singlet-triplet transitions are important.

Contrary to the multiband p - d model's parameters that fall with distance rapidly, effective model parameters do not decrease so fast. This happens due to weak distance dependence of Wannier functions that determine coefficients²⁸ μ_{fg}^z , ν_{fg} , λ_{fg} , ξ_{fg} , χ_{fg} which, in turn, determine distance dependence of effective model parameters (15).

To demonstrate the importance of hoppings to far coordination spheres (c.s.) in Fig. 9 we present the dispersion and DOS in the t - J^* model with parameters from Table IV. The electron Green function (17) has been calculated beyond the Hubbard-I approximation by a decoupling of static correlation functions that includes short-range magnetic order: $\langle X_f^{\sigma\sigma} X_g^{\sigma'\sigma'} \rangle \rightarrow n_p^2 + (\sigma/\sigma') \frac{1}{2} C_{fg}$, $\langle X_f^{\sigma\bar{\sigma}} X_g^{\bar{\sigma}\sigma} \rangle = C_{fg}$. Here n_p is the occupation factors of the single-particle state, $C_{fg} = 2 \langle S_f^z S_g^z \rangle$ are static spin correlation functions which were self-

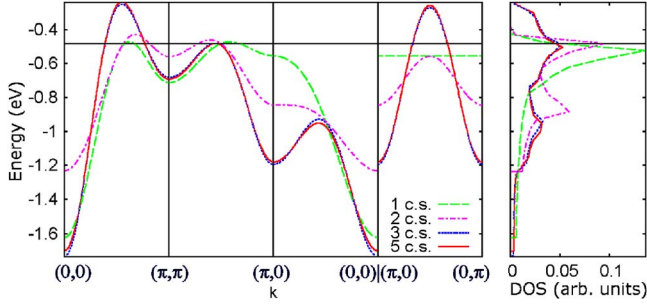


FIG. 9. (Color online) Quasiparticle dispersion and corresponding densities of states (DOS) in the $t\text{-}J^*$ model calculated for different number of taken into account coordination spheres (c.s.). Chemical potential shown by the straight horizontal line was calculated self-consistently assuming 15% holes doping.

consistently calculated from the spin Green's functions in the 2D $t\text{-}J$ model.⁸⁰ As one can easily see from Fig. 9, the dispersion with hoppings only to nearest neighbors (1 c.s.) and to next-nearest neighbors (2 c.s., the so called $t\text{-}t'\text{-}J^*$ model) is quantitatively different around $(0, 0)$ point and *qualitatively* different around $(\pi, 0)$ point from the dispersion with 3 c.s. ($t\text{-}t'\text{-}t''\text{-}J^*$ model) and more coordination spheres taken into account.

Recent ARPES experiments⁸¹ show that the Fermi velocity $v_F = E_F/k_F$ is nearly constant for wide range of p -type materials and doping independent within an experimental error of 20%. We have calculated this quantity in the $t\text{-}J^*$ model with parameters from Table IV in the approximation described above. In the doping range from $x=0.03$ to $x=0.15$ our calculations give very weak doping dependence of the Fermi velocity. Assuming the lattice constant equal to 4 Å we have v_F varying from 1.6 to 2.0 eV Å⁻¹. Taking into account experimental error of 20% our results are very close to the experimental one.

VI. CONCLUSION

The approach developed here assumes the multiband Hamiltonian for the real crystal structure and its mapping onto low-energy model. Parameters of the effective model (15) are obtained directly from *ab initio* multiband model parameters. The sets of parameters for the effective models (23) and (24) are presented in Tables IV and V for p - and n -type cuprates, correspondingly.

The effective low-energy model appears to be the $t\text{-}t'\text{-}t''\text{-}J^*$ model (23) for Nd₂CuO₄ and the singlet-triplet $t\text{-}t'\text{-}t''\text{-}J^*$ model (24) for La₂CuO₄. There is almost no difference in the band dispersion with addition of numerically small hoppings to fourth, fifth, etc., neighbors. Summarizing, we have shown that the hybrid LDA+GTB method incorporates the *ab initio* calculated parameters of the multiband $p\text{-}d$ model and the adequate treatment of strong electron correlations.

ACKNOWLEDGMENTS

The authors would like to thank A.V. Sherman for very helpful discussions. This work was supported by Joint Integration Program of Siberian and Ural Branches of Russian Academy of Sciences, Netherlands Organization for Scientific Research through NWO Grant No. 047.016.005, RFBR Grant Nos. 05-02-16301, 04-02-16096, 03-02-16124, and 05-02-17244, RFBR-GFEN Grant No. 03-02-39024, program of the Presidium of the Russian Academy of Sciences (RAS) "Quantum macrophysics." Z.P. and I.N. acknowledge support from the Dynasty Foundation and International Centre for Fundamental Physics in Moscow, Russian Science Support Foundation.

APPENDIX: EXPRESSIONS FOR THREE-CENTER CORRELATED HOPPINGS IN EFFECTIVE MODELS

In the $t\text{-}J^*$ model (23) the three-center correlated hoppings are given by

$$H_3 = \frac{t_{fm}^{0S} t_{mg}^{0S}}{E_{ct}} (X_f^{\sigma 0} X_m^{\bar{\sigma} \sigma} X_g^{0 \bar{\sigma}} - X_f^{\sigma 0} X_m^{\bar{\sigma} \bar{\sigma}} X_g^{0 \sigma}). \quad (\text{A1})$$

The three-center interaction terms $H_{\text{eff}3}$ in the effective Hamiltonian (24) are much more complicated than in the $t\text{-}J^*$ model due to additional triplet and singlet-triplet contributions:

$$H_{\text{eff}3} = \frac{t_{fm}^{0S} t_{mg}^{0S}}{E_{ct}} H_3^{SS} - v \frac{t_{fm}^{0S} t_{mg}^{ST}}{E_{ct}} H_3^{ST} + v \frac{t_{fm}^{ST} t_{mg}^{ST}}{E_{ct}} H_3^{TT},$$

$$H_3^{SS} = (X_f^{\sigma S} X_m^{\bar{\sigma} \sigma} X_g^{S \bar{\sigma}} - X_f^{\bar{\sigma} S} X_m^{\sigma \sigma} X_g^{S \bar{\sigma}}),$$

$$\begin{aligned} H_3^{ST} = & \frac{1}{\sqrt{2}} (X_f^{\sigma T 0} X_m^{\bar{\sigma} \sigma} X_g^{T 0 \bar{\sigma}} - X_f^{\bar{\sigma} T 0} X_m^{\sigma \sigma} X_g^{T 0 \bar{\sigma}}) \\ & + 2\sigma (X_f^{\bar{\sigma} T 2 \bar{\sigma}} X_m^{\bar{\sigma} \sigma} X_g^{T 2 \sigma \bar{\sigma}} + X_f^{\sigma T 2 \sigma} X_m^{\sigma \sigma} X_g^{T 2 \sigma \bar{\sigma}}) \\ & + \frac{1}{\sqrt{2}} (X_f^{\sigma S} X_m^{\bar{\sigma} \sigma} X_g^{T 0 \bar{\sigma}} - X_f^{\bar{\sigma} S} X_m^{\sigma \sigma} X_g^{T 0 \bar{\sigma}}) \\ & - 2\sigma (X_f^{\sigma S} X_m^{\bar{\sigma} \sigma} X_g^{T 2 \sigma \sigma} - X_f^{\bar{\sigma} S} X_m^{\sigma \sigma} X_g^{T 2 \sigma \sigma}), \end{aligned}$$

$$\begin{aligned} H_3^{TT} = & \frac{1}{2} (X_f^{\sigma T 0} X_m^{\bar{\sigma} \sigma} X_g^{T 0 \bar{\sigma}} - X_f^{\bar{\sigma} T 0} X_m^{\sigma \sigma} X_g^{T 0 \bar{\sigma}}) \\ & - (X_f^{\bar{\sigma} T 2 \bar{\sigma}} X_m^{\bar{\sigma} \sigma} X_g^{T 2 \sigma \sigma} + X_f^{\sigma T 2 \sigma} X_m^{\sigma \sigma} X_g^{T 2 \sigma \sigma}) \\ & + \frac{2\sigma}{\sqrt{2}} (-X_f^{\sigma T 0} X_m^{\bar{\sigma} \sigma} X_g^{T 2 \sigma \sigma} + X_f^{\bar{\sigma} T 0} X_m^{\sigma \sigma} X_g^{T 2 \sigma \sigma}) \\ & + \frac{2\sigma}{\sqrt{2}} (+X_f^{\bar{\sigma} T 2 \bar{\sigma}} X_m^{\bar{\sigma} \sigma} X_g^{T 0 \bar{\sigma}} + X_f^{\sigma T 2 \sigma} X_m^{\sigma \sigma} X_g^{T 0 \bar{\sigma}}). \quad (\text{A2}) \end{aligned}$$

*Electronic address: mkor@iph.krasn.ru

†Electronic address: pzv@optics.imp.uran.ru

- ¹P. Hohenberg and W. Kohn, Phys. Rev. **136**, 864 (1964).
- ²W. Kohn and L. J. Sham, Phys. Rev. **140**, 1133 (1965).
- ³V. I. Anisimov, J. Zaanen, and O. K. Andersen, Phys. Rev. B **44**, 943 (1991).
- ⁴A. Svane and O. Gunnarsson, Phys. Rev. Lett. **65**, 1148 (1990).
- ⁵J. C. Hubbard, Proc. R. Soc. London, Ser. A **276**, 238 (1963).
- ⁶V. I. Anisimov, A. I. Poteryaev, M. A. Korotin, A. O. Anokhin, and G. Kotliar, J. Phys.: Condens. Matter **35**, 7359 (1997).
- ⁷K. Held, I. A. Nekrasov, N. Blümer, V. I. Anisimov, and D. Vollhardt, Int. J. Mod. Phys. B **15**, 2611 (2001); K. Held, I. A. Nekrasov, G. Keller, V. Eyert, N. Blümer, A. K. McMahan, R. T. Scalettar, T. Pruschke, V. I. Anisimov, and D. Vollhardt, in *Quantum Simulations of Complex Many-Body Systems: From Theory to Algorithms*, edited by J. Grotendorst, D. Marks and A. Muramatsu, Vol. 10 of *NIC Series* (NIC Directors, Forschungszentrum Jülich, Jülich, 2002), p. 175–209.
- ⁸K. Held, I. A. Nekrasov, G. Keller, V. Eyert, N. Blümer, A. K. McMahan, R. T. Scalettar, Th. Pruschke, V. I. Anisimov, and D. Vollhardt, psi-k.dl.ac.uk/newsletters/News_56/Highlight_56.pdf.
- ⁹A. I. Lichtenstein and M. I. Katsnelson, Phys. Rev. B **57**, 6884 (1998).
- ¹⁰D. Vollhardt, in *Correlated Electron Systems*, edited by V. J. Emery (World Scientific, Singapore, 1993), p. 57.
- ¹¹G. Kotliar and D. Vollhardt, Phys. Today **57**, 53 (2004).
- ¹²W. Metzner and D. Vollhardt, Phys. Rev. Lett. **62**, 324 (1989).
- ¹³A. Georges, G. Kotliar, W. Krauth, and M. Rozenberg, Rev. Mod. Phys. **68**, 13 (1996).
- ¹⁴M. H. Hettler, A. N. Tahvildar-Zadeh, M. Jarrell, T. Pruschke, and H. R. Krishnamurthy, Phys. Rev. B **58**, R7475 (1998).
- ¹⁵Th. Maier, M. Jarrell, Th. Pruschke, and M. Hettler, cond-mat/0404055 (unpublished).
- ¹⁶S. Yu. Savrasov and G. Kotliar, Phys. Rev. B **69**, 245101 (2004).
- ¹⁷L. Hedin, Phys. Rev. **139**, A796 (1965).
- ¹⁸R. Del Sole, L. Reining, and R. W. Godby, Phys. Rev. B **49**, 8024 (1994).
- ¹⁹R. W. Godby, M. Schlüter, and L. J. Sham, Phys. Rev. Lett. **56**, 2415 (1986).
- ²⁰F. Aryasetiawan and O. Gunnarsson, Phys. Rev. Lett. **74**, 3221 (1995).
- ²¹S. V. Faleev, M. van Schilfgaarde, and T. Kotani, Phys. Rev. Lett. **93**, 126406 (2004).
- ²²S. G. Ovchinnikov and I. S. Sandalov, Physica C **161**, 607 (1989).
- ²³V. J. Emery, Phys. Rev. Lett. **58**, 2794 (1987).
- ²⁴C. M. Varma, S. Smitt-Rink, and E. Abrahams, Solid State Commun. **62**, 681 (1987).
- ²⁵S. V. Lovtsov and V. Yu. Yushankhai, Physica C **179**, 159 (1991).
- ²⁶J. H. Jefferson, H. Eskes, and L. F. Feiner, Phys. Rev. B **45**, 7959 (1992).
- ²⁷H.-B. Schüttler and A. J. Fedro, Phys. Rev. B **45**, 7588 (1992).
- ²⁸V. A. Gavrichkov, S. G. Ovchinnikov, A. A. Borisov, and E. G. Goryachev, Zh. Eksp. Teor. Fiz. **118**, 422 (2000); [JETP **91**, 369 (2000)].
- ²⁹V. Gavrichkov, A. Borisov, and S. G. Ovchinnikov, Phys. Rev. B **64**, 235124 (2001).
- ³⁰V. A. Gavrichkov, S. G. Ovchinnikov, and L. E. Yakimov (unpublished).
- ³¹S. G. Ovchinnikov and O. G. Petrakovsky, J. Supercond. **4**, 437 (1991).
- ³²G. H. Wannier, Phys. Rev. **52**, 191 (1937).
- ³³N. Marzari and D. Vanderbilt, Phys. Rev. B **56**, 12847 (1997).
- ³⁴Wei Ku, H. Rosner, W. E. Pickett, and R. T. Scalettar, Phys. Rev. Lett. **89**, 167204 (2002).
- ³⁵O. K. Andersen and O. Jepsen, Phys. Rev. Lett. **53**, 2571 (1984).
- ³⁶V. I. Anisimov, D. E. Kondakov, A. V. Kozhevnikov, I. A. Nekrasov, Z. V. Pchelkina, J. W. Allen, S.-K. Mo, H.-D. Kim, P. Metcalf, S. Suga, A. Sekiyama, G. Keller, I. Leonov, X. Ren, and D. Vollhardt, Phys. Rev. B **71**, 125119 (2005).
- ³⁷H. Wilhelm, C. Cros, E. Reny, G. Demazeau, and M. Hanfland, J. Mater. Chem. **8**, 2729 (1998).
- ³⁸P. G. Radaelli, D. G. Hinks, A. W. Mitchell, B. A. Hunter, J. L. Wagner, B. Dabrowski, K. G. Vandervoort, H. K. Viswanathan, and J. D. Jorgensen, Phys. Rev. B **49**, 4163 (1994).
- ³⁹T. Kamiyama, F. Izumi, H. Takahashi, J. D. Jorgensen, B. Dabrowski, R. L. Hitterman, D. G. Hinks, H. Shakéd, T. O. Mason, and M. Seabaugh, Physica C **229**, 377 (1994).
- ⁴⁰O. K. Andersen, Z. Pawłowska, and O. Jepsen, Phys. Rev. B **34**, 5253 (1986).
- ⁴¹O. Gunnarsson, O. K. Andersen, O. Jepsen, and J. Zaanen, Phys. Rev. B **39**, 1708 (1989); V. I. Anisimov and O. Gunnarsson, *ibid.* **43**, 7570 (1991).
- ⁴²V. I. Anisimov, M. A. Korotin, I. A. Nekrasov, Z. V. Pchelkina, and S. Sorella, Phys. Rev. B **66**, 100502(R) (2002).
- ⁴³Yu. Gaididei and V. Loktev, Phys. Status Solidi B **147**, 307 (1988).
- ⁴⁴A. Bianconi, M. De Santis, A. Di Cicco, A. M. Flank, A. Fontaine, P. Lagarde, H. Katayama-Yoshida, A. Kotani, and A. Marcelli, Phys. Rev. B **38**, 7196 (1988).
- ⁴⁵H. Romberg, N. Nücker, M. Alexander, J. Fink, D. Hahn, T. Zetterer, H. H. Otto, and K. F. Renk, Phys. Rev. B **41**, 2609 (1990).
- ⁴⁶C. T. Chen, L. H. Tjeng, J. Kwo, H. L. Kao, P. Rudolf, F. Sette, and R. M. Fleming, Phys. Rev. Lett. **68**, 2543 (1992).
- ⁴⁷R. Raimondi, J. H. Jefferson, and L. F. Feiner, Phys. Rev. B **53**, 8774 (1996).
- ⁴⁸J. C. Hubbard, Proc. R. Soc. London, Ser. A **277**, 237 (1964).
- ⁴⁹M. M. Korshunov, V. A. Gavrichkov, S. G. Ovchinnikov, Z. V. Pchelkina, I. A. Nekrasov, M. A. Korotin, and V. I. Anisimov, Zh. Eksp. Teor. Fiz. **126**, 642 (2004) [JETP **99**, 559 (2004)].
- ⁵⁰M. M. Korshunov, V. A. Gavrichkov, S. G. Ovchinnikov, D. Manske, and I. Eremin, Physica C **402**, 365 (2004).
- ⁵¹B. O. Wells, Z.-X. Shen, A. Matsuura, D. M. King, M. A. Kastner, M. Greven, and R. J. Birgeneau, Phys. Rev. Lett. **74**, 964 (1995).
- ⁵²C. Dürr, S. Legner, R. Hayn, S. V. Borisenko, Z. Hu, A. Theresiak, M. Knupfer, M. S. Golden, J. Fink, F. Ronning, Z.-X. Shen, H. Eisaki, S. Uchida, C. Janowitz, R. Müller, R. L. Johnson, K. Rossnagel, L. Kipp, and G. Reichardt, Phys. Rev. B **63**, 014505 (2000).
- ⁵³A. A. Borisov, V. A. Gavrichkov, and S. G. Ovchinnikov, Mod. Phys. Lett. B **17**, 479 (2003).
- ⁵⁴A. A. Borisov, V. A. Gavrichkov, and S. G. Ovchinnikov, Zh. Eksp. Teor. Fiz. **124**, 862 (2003); [JETP **97**, 773 (2003)].
- ⁵⁵A. Ino, T. Mizokawa, A. Fujimori, K. Tamasaku, H. Eisaki, S. Uchida, T. Kimura, T. Sasagawa, and K. Kishio, Phys. Rev. Lett. **79**, 2101 (1997).
- ⁵⁶N. Harima, J. Matsuno, A. Fujimori, Y. Onose, Y. Taguchi, and Y. Tokura, Phys. Rev. B **64**, 220507(R) (2001).

- ⁵⁷A. Ino, C. Kim, M. Nakamura, T. Yoshida, T. Mizokawa, A. Fujimori, Z.-X. Shen, T. Kakeshita, H. Eisaki, and S. Uchida, *Phys. Rev. B* **65**, 094504 (2002).
- ⁵⁸N. P. Armitage, D. H. Lu, C. Kim, A. Damascelli, K. M. Shen, F. Ronning, D. L. Feng, P. Bogdanov, Z.-X. Shen, Y. Onose, Y. Taguchi, Y. Tokura, P. K. Mang, N. Kaneko, and M. Greven, *Phys. Rev. Lett.* **87**, 147003 (2001).
- ⁵⁹R. O. Zaitsev, *Sov. Phys. JETP* **41**, 100 (1975).
- ⁶⁰Yu. Izumov and B. M. Letfullov, *J. Phys.: Condens. Matter* **3**, 5373 (1991).
- ⁶¹S. G. Ovchinnikov and V. V. Val'kov, *Hubbard Operators in the Theory of Strongly Correlated Electrons* (Imperial College Press, London, 2004).
- ⁶²V. G. Bar'yakhtar, V. N. Krivoruchko, and D. A. Yablonskii, *Green's Functions in Magnetism Theory* (Naukau Dumka, Kiev, 1984) [in Russian].
- ⁶³O. K. Andersen, A. I. Liechtenstein, O. Jepsen, and F. Paulsen, *J. Phys. Chem. Solids* **56**, 1573 (1995).
- ⁶⁴E. Pavarini, I. Dasgupta, T. Saha-Dasgupta, O. Jepsen, and O. K. Andersen, *Phys. Rev. Lett.* **87**, 047003 (2001).
- ⁶⁵A. S. Moskvina, J. Ma'lek, M. Knupfer, R. Neudert, J. Fink, R. Hayn, S.-L. Drechsler, N. Motoyama, H. Eisaki, and S. Uchida, *Phys. Rev. Lett.* **91**, 037001 (2003).
- ⁶⁶A. S. Moskvina, *Pis'ma Zh. Eksp. Teor. Fiz.* **80**, 824 (2004) [*JETP Lett.* **80**, 697 (2004)].
- ⁶⁷T. Tohyama and S. Maekawa, *Phys. Rev. B* **49**, 3596 (1994).
- ⁶⁸S. G. Ovchinnikov, A. A. Borisov, V. A. Gavrichkov, and M. M. Korshunov, *J. Phys.: Condens. Matter* **16**, L93 (2004).
- ⁶⁹D. Vaknin, S. K. Sinha, D. E. Moncton, D. C. Johnston, J. M. Newsam, C. R. Safinya, and H. E. King, Jr., *Phys. Rev. Lett.* **58**, 2802 (1987).
- ⁷⁰J. M. Tranquada, A. H. Moudden, A. I. Goldman, P. Zolliker, D. E. Cox, G. Shirane, S. K. Sinha, D. Vaknin, D. C. Johnston, M. S. Alvarez, A. J. Jacobson, J. T. Lewandowski, and J. M. Newsam, *Phys. Rev. B* **38**, 2477 (1988).
- ⁷¹T. Freltoft, G. Shirane, S. Mitsuda, J. P. Remeika, and A. S. Cooper, *Phys. Rev. B* **37**, 137 (1988).
- ⁷²P. Horsch and W. von der Linden, *Z. Phys. B: Condens. Matter* **72**, 181 (1988).
- ⁷³A. A. Katanin and A. P. Kampf, *Phys. Rev. B* **66**, 100403(R) (2003).
- ⁷⁴L. N. Bulaevskii, E. L. Nagaev, and D. I. Khomskii, *Sov. Phys. JETP* **54**, 1562 (1968).
- ⁷⁵K. A. Chao, J. Spalek, and A. M. Oles, *J. Phys. C* **10**, 271 (1977).
- ⁷⁶J. E. Hirsch, *Phys. Rev. Lett.* **54**, 1317 (1985).
- ⁷⁷F. C. Zhang and T. M. Rice, *Phys. Rev. B* **41**, 7243 (1990).
- ⁷⁸V. I. Belinicher and A. L. Chernyshev, *Phys. Rev. B* **47**, 390 (1993).
- ⁷⁹L. F. Feiner, J. H. Jefferson, and R. Raimondi, *Phys. Rev. B* **53**, 8751 (1996).
- ⁸⁰A. Sherman and M. Schreiber, *Eur. Phys. J. B* **32**, 203 (2003).
- ⁸¹X. J. Zhou, T. Yoshida, A. Lanzara, P. V. Bogdanov, S. A. Kellar, K. M. Shen, W. L. Yang, F. Ronning, T. Sasagawa, T. Kakeshita, T. Noda, H. Eisaki, S. Uchida, C. T. Lin, F. Zhou, J. W. Xiong, W. X. Ti, Z. X. Zhao, A. Fujimori, Z. Hussain, and Z.-X. Shen, *Nature (London)* **423**, 398 (2003).